Applied Physics Reviews

Giant bulk spin–orbit torque and efficient electrical switching in single ferrimagnetic FeTb layers with strong perpendicular magnetic anisotropy

Cite as: Appl. Phys. Rev. **9**, 021402 (2022); https://doi.org/10.1063/5.0087260
Submitted: 03 February 2022 • Accepted: 25 March 2022 • Published Online: 07 April 2022

Qianbiao Liu, Lijun Zhu, Xiyue S. Zhang, et al.

COLLECTIONS

This paper was selected as Featured

View Online Export Citation CrossMark

ARTICLES YOU MAY BE INTERESTED IN

Efficient and controllable magnetization switching induced by intermixing-enhanced bulk spin–orbit torque in ferromagnetic multilayers
Applied Physics Reviews **9**, 011407 (2022); https://doi.org/10.1063/5.0067348

Van der Waals epitaxy growth of 2D ferromagnetic $Cr_{(1+\delta)}Te_2$ nanolayers with concentration-tunable magnetic anisotropy
Applied Physics Reviews **9**, 011409 (2022); https://doi.org/10.1063/5.0070079

Large unidirectional spin Hall and Rashba–Edelstein magnetoresistance in topological insulator/magnetic insulator heterostructures
Applied Physics Reviews **9**, 011406 (2022); https://doi.org/10.1063/5.0073976

AIP Publishing Applied Physics Reviews
Read. Cite. Publish. Repeat.
19.162
2020 IMPACT FACTOR*

AIP Publishing

© 2022 Author(s).

Applied Physics Reviews ARTICLE scitation.org/journal/are

Giant bulk spin–orbit torque and efficient electrical switching in single ferrimagnetic FeTb layers with strong perpendicular magnetic anisotropy

Cite as: Appl. Phys. Rev. **9**, 021402 (2022); doi: 10.1063/5.0087260
Submitted: 3 February 2022 · Accepted: 25 March 2022 ·
Published Online: 7 April 2022

View Online Export Citation CrossMark

Qianbiao Liu,[1,2] Lijun Zhu,[1,2,a)] Xiyue S. Zhang,[2] David A. Muller,[2] and Daniel C. Ralph[2,3]

AFFILIATIONS

[1]State Key Laboratory of Superlattices and Microstructures, Institute of Semiconductors, Chinese Academy of Sciences, Beijing 100083, China
[2]Cornell University, Ithaca, New York 14850, USA
[3]Kavli Institute at Cornell, Ithaca, New York 14850, USA

[a)]**Author to whom correspondence should be addressed:** ljzhu@semi.ac.cn

ABSTRACT

Efficient manipulation of antiferromagnetically coupled materials that are integration-friendly and have strong perpendicular magnetic anisotropy (PMA) is of great interest for low-power, fast, dense magnetic storage and computing. Here, we report a distinct, giant bulk damping-like spin–orbit torque in strong-PMA ferrimagnetic $Fe_{100-x}Tb_x$ single layers that are integration-friendly (composition-uniform, amorphous, and sputter-deposited). For sufficiently thick layers, this bulk torque is constant in the efficiency per unit layer thickness, ξ^j_{DL}/t, with a record-high value of $0.036 \pm 0.008\ nm^{-1}$, and the damping-like torque efficiency ξ^j_{DL} achieves very large values for thick layers, up to 300% for 90 nm layers. This giant bulk torque by itself switches tens of nm thick $Fe_{100-x}Tb_x$ layers that have very strong PMA and high coercivity at current densities as low as a few MA/cm^2. Surprisingly, for a given layer thickness, ξ^j_{DL} shows strong composition dependence and becomes negative for composition where the total angular momentum is oriented parallel to the magnetization rather than antiparallel. Our findings of giant bulk spin torque efficiency and intriguing torque-compensation correlation will stimulate study of such unique spin–orbit phenomena in a variety of ferrimagnetic hosts. This work paves a promising avenue for developing ultralow-power, fast, dense ferrimagnetic storage and computing devices.

Published under an exclusive license by AIP Publishing. https://doi.org/10.1063/5.0087260

INTRODUCTION

Ferrimagnetic materials can host a variety of exotic properties that are promising for technology, e.g., magnetization/angular momentum compensation, giant perpendicular magnetic anisotropy (PMA),[1–4] ultrafast magnetic domain wall velocities,[5–7] reduced sensitivity to stray magnetic fields than ferromagnets, and easier and fast detection than antiferromagnets. Therefore, ferrimagnets (FIMs) are potentially advantageous for dense and fast magnetic recording, memory, and computing applications.[8,9] However, successful integration of FIMs into high-performance functional devices requires efficient manipulation of strong-PMA and integration-friendly FIMs, which has remained a big challenge. So far, electrical switching of FIMs by interfacial spin–orbit torque (SOT)[11] is only reported in samples with poor PMA, small coercivities (e.g., $H_c < 0.2$ kOe for GdFeCo[3,10,12] $H_c < 0.25$ kOe for CoTb[13,14]), and low SOT efficiencies ($\xi^j_{DL} = 0.017$ for Pt/CoTb[15]). Moreover, the yet-known bulk SOTs[16–22] in magnetic single layers have low efficiency per unit film thickness[20–27] and/or usually require a single-crystal structure[17] and a composition gradient,[16,18,19,22] which limit practical application.

Here, we report a record-strong bulk SOT within single layers of $Fe_{100-x}Tb_x$ alloys (FeTb for short) that have strong PMA, spatially uniform, amorphous structure, and are grown simply by sputtering onto oxidized silicon substrates, which are highly desirable for large-scale and high-density integration with CMOS circuits. Surprisingly, the efficiency of the bulk torque varies rapidly as a function of stoichiometry and reverses sign in between the compensation points for magnetization and angular momentum. We also show that this bulk SOT can switch tens of nm thick FeTb layers with strong PMA and high H_c at extremely low current densities.

SAMPLE CHARACTERIZATIONS

For this work, we deposit a series of $Fe_{100-x}Tb_x$ single layers with different thicknesses and Tb volume percentages ($x = 15$–78) by co-sputtering at room temperature. Each sample is capped by a MgO

(1.6 nm)/Ta (1.6 nm) bilayer that is fully oxidized upon exposure to the atmosphere [see the electron energy loss spectrum (EELS) results in Ref. 26]. For measurements of SOT and SOT-induced switching, the layers are patterned into Hall bars that are 60 μm long and 5 μm wide. More details about sample preparation and characterization can be found in the supplementary material, Sec. 1. These FeTb alloys have an amorphous and homogeneous texture and reasonably sharp interfaces, as indicated by cross-sectional scanning transmission electron microscopy (STEM) measurements [see Fig. 1(a) for the example of a $Fe_{57}Tb_{43}$ sample (66 nm)]. EELS measurements demonstrate that there is no obvious variation in the ratio of Fe to Tb concentrations through the thickness of the films [Fig. 1(b)]. There is an overall variation in the absolute EELS intensities of Fe and Tb due to variations in thickness along the sample wedge created during the ion-beam thinning process (see the supplementary material, Sec. 2 and Ref. 27), but this should not be misinterpreted as a composition gradient. There is also no obvious indication of oxidization of the FeTb from the EELS imaging, which consists with the previous observation[16] that the MgO (1.6 nm)/Ta (1.6 nm) bilayer well protects the magnetic layers from oxidization.

The FeTb samples have strong PMA and square perpendicular magnetization hysteresis loops over a wide composition range, $x = 29$–61, when the thickness is greater than 7 nm [Fig. 1(c) and the supplementary material, Fig. S3]. The perpendicular magnetic anisotropy field (H_k) is very high and reaches values as large as 100 kOe for 20 nm films near $x = 47$ [Fig. 1(d)]. In Figs. 1(e)–1(g), we summarize the saturation magnetization (M_s), the coercivity (H_c), and the anomalous Hall resistance (R_{AHE}) for 20 nm $Fe_{100-x}Tb_x$ samples as a function of x. As expected, M_s shows a strong, "V-shaped" variation with x, which is a characteristic of the competing magnetic moment contributions of the antiparallel Fe and Tb sub-lattices. From the fit of the data to the relation $M_s = (1 - 0.01x)\, M_{Fe} - 0.01x\, M_{Tb}$ [see the orange solid line in Fig. 1(e)], we obtain $M_{Fe} = 824 \pm 40$ emu/cm^3 ($\approx$1.05 μ_B) and $M_{Tb} = 940 \pm 80$ emu/cm^3 ($\approx$3.14 μ_B) of our samples. The values of M_{Fe} and M_{Tb} of our disordered thin films are smaller than typical bulk values (i.e., 2.20 μ_B/Fe or 9.72 μ_B/Tb[8]). The magnetization compensation point ($x_M \approx 47$ for our 20 nm FeTb samples at room temperature), at which M_s vanishes and H_c appears to diverge, also differs from previously reported values for 20 nm FeTb grown on Pt ($x_M \approx 25$).[28–30] However, it is common that the magnetic properties of thin films of

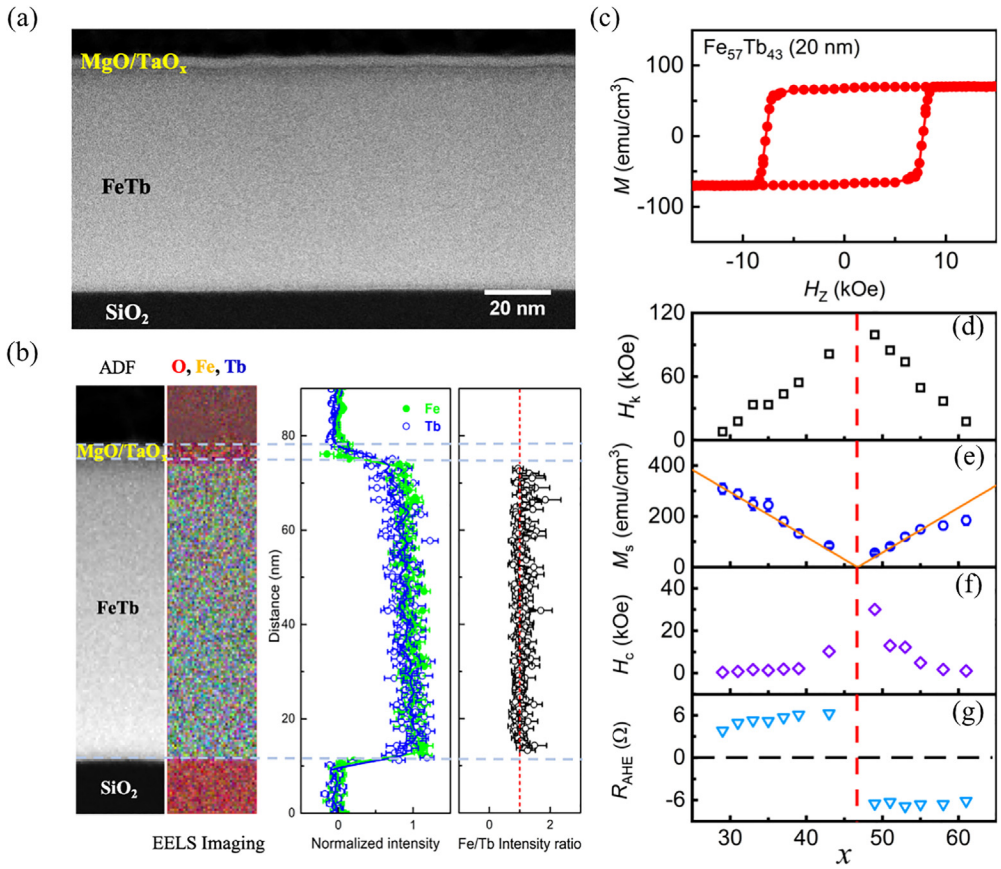

FIG. 1. Sample characterizations. (a) High-angle dark-field cross-sectional STEM image. (b) Depth profile of the EELS intensity for O, Fe, and Tb, showing the absence of any composition gradient in the $Fe_{57}Tb_{43}$ layer. (c) Out-of-plane magnetization curve for the 20 nm $Fe_{57}Tb_{43}$ sample. (d) Perpendicular magnetic anisotropy field (H_k), (e) saturation magnetization (M_s), (f) coercivity (H_c), and (g) anomalous Hall resistance (R_{AHE}) of $Fe_{100-x}Tb_x$ films with varying Tb concentration (x). Here, the values of H_k, H_c, and R_{AHE} are determined from transport measurements.

Published under an exclusive license by AIP Publishing

ferrimagnetic alloys can vary depending on growth protocols and substrate choices. For example, x_M of CoTb at room temperature has been reported to be ≈22,[13] ≈35,[31] and ≈44[32] when the CoTb is grown on Ta, Pt, and SiN, respectively. We also observe that the magnetic properties of our FeTb samples are sensitive to the layer thickness [supplementary material, Figs. S3(c)–S3(e)], in line with previous reports.[30] As expected, R_{AHE} for the 20 nm FeTb is positive for $x < x_M$ but negative for $x > x_M$ [see the supplementary material, Fig. S4(a) for more details] because when $x < x_M$ ($x > x_M$), the Fe moment is parallel (antiparallel) to the total magnetization and to a strong applied perpendicular magnetic field (H_z). The 3*d* states of Fe govern the anomalous Hall effect because the 4*f* states of Tb are expected to be located well below the Fermi level and are less involved in transport phenomena of FeTb.

GIANT BULK SPIN–ORBIT TORQUE

We measure the efficiencies of SOTs in the perpendicularly magnetized FeTb samples using the polar-angle dependent harmonic Hall voltage response (HHVR) technique[33,34] after carefully taking into account current-induced heating and thermoelectric effects (supplementary material, Secs. 5 and 6). This HHVR technique is accurate when the magnetization rotates coherently at small polar angles (θ_M). This condition is fulfilled in the FeTb samples, as indicated by a well-defined parabolic scaling of the first harmonic Hall signal vs θ_M (supplementary material, Fig. S8). To determine the dampinglike SOT, we rotate the magnetization by scanning a fixed magnitude of magnetic field (H_{xz}) relative to the sample at small values of θ_M in the *x*–*z* plane [Fig. 2(a)] and collect the first and the second HHVRs, V_ω and $V_{2\omega}$, as a function of θ_M under the excitation of a low-frequency sinusoidal electric field *E* in the *x* direction. As we discuss in detail in the supplementary material, Sec. 6, the HHVR signals are given by

$$V_\omega = V_{AHE}\cos\theta_M, \tag{1}$$

$$V_{2\omega} \approx \left(\frac{1}{2}V_{AHE}\frac{H_{DL}}{H_k + H_{xz}} + V_{ANE,z}\right)\sin\theta_M + V_{ANE,x}, \tag{2}$$

where V_{AHE} is the anomalous Hall voltage, $V_{ANE,z(x)}$ is the anomalous Nernst voltage induced by an out-of-plane (in-plane) temperature gradient, and H_{DL} is the damping-like effective SOT field. As shown in Fig. 2(b), the measured $V_{2\omega}$ varies linearly with $\sin\theta_M$ for each fixed magnitude of H_{xz}. The value of H_{DL} can be obtained from the fits of data to Eq. (2) as shown in Fig. 2(c). In this determination, we ignore the so-called "planar Hall correction"[35] because the planar Hall resistance (R_{PHE}) samples are negligibly small compared to R_{AHE} ($|R_{PHE}/R_{AHE}| \leq 0.04$, supplementary material, Fig. S9), and even if this were not the case, the planar Hall correction is generally found to give incorrect values when it is not negligible.[36–38] As shown in Fig. 2(d), H_{DL} for the FeTb single layers with different *x* increases much more slowly than $1/M_s$ scaling upon approaching the magnetization

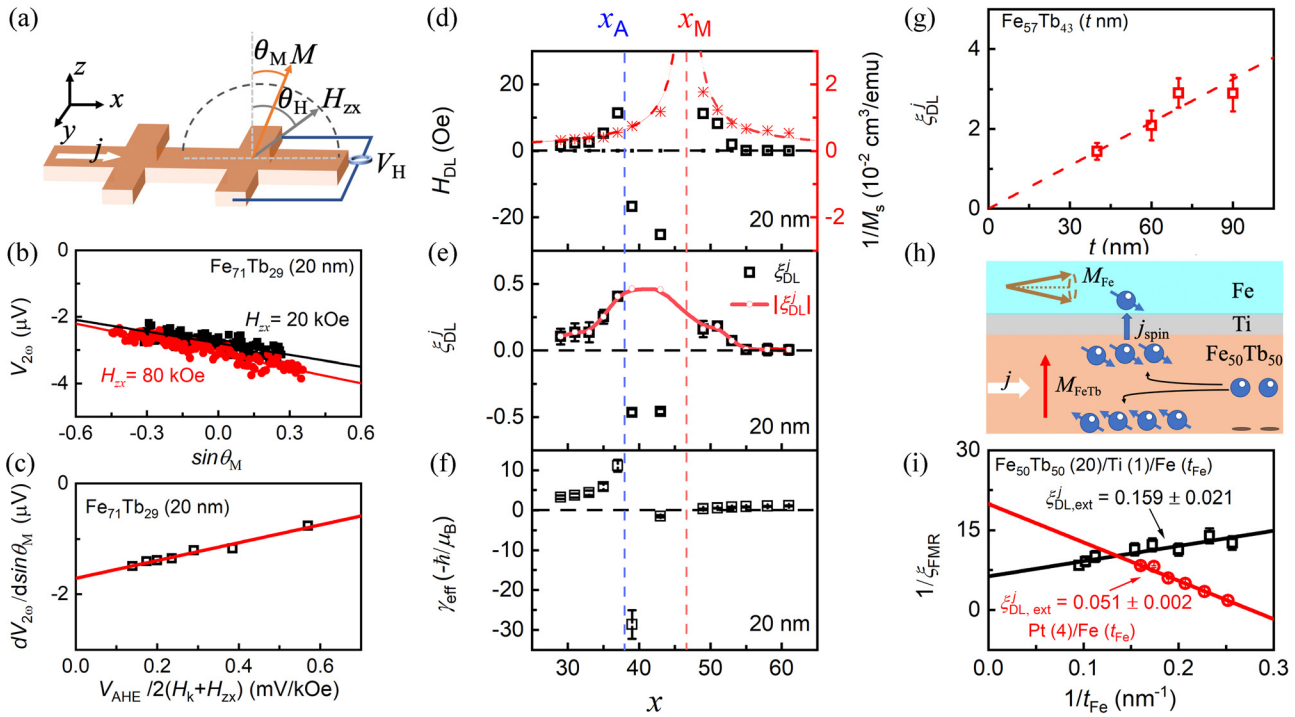

FIG. 2. Spin–orbit torques. (a) Geometry of the HHVR measurement. (b) Second HHVR $V_{2\omega}$ vs $\sin\theta_M$ for a 20 nm $Fe_{71}Tb_{29}$ sample for constant magnitudes of applied magnetic fields $H_{zx} = 20$ and 80 kOe. (c) $dV_{2\omega}/d\sin\theta_M$ vs $V_{AHE}/2(H_k+H_{zx})$ for 20 nm $Fe_{71}Tb_{29}$. Dependence on the Tb concentration *x* for (d) the damping-like effective SOT field H_{DL}, (e) the damping-like torque efficiencies per current density ξ^j_{DL} and $|\xi^j_{DL}|$, and (f) the calculated value of γ_{eff} for the 20 nm $Fe_{100-x}Tb_x$. In (d)–(f), the dashed lines indicate the angular momentum compensation point x_A (blue dashed line) and the magnetization compensation point x_M (red dashed line). (g) ξ^j_{DL} vs the thickness (*t*) of $Fe_{47}Tb_{43}$ samples [$\xi^j_{DL} > 0$ because the composition $x = 43$ is located in the Tb-dominated regime when the thickness is greater than ≈30 nm, see the supplementary material, Fig. S4(e)]. (h) Schematic of ST-FMR measurements on $Fe_{50}Tb_{50}$ (20 nm)/Ti (1 nm)/Fe (t_{Fe}) samples. (i) Inverse FMR efficiency ($1/\xi_{FMR}$) vs inverse Fe thickness ($1/t_{Fe}$) for the $Fe_{50}Tb_{50}$ (20 nm)/Ti (1 nm)/Fe (t_{Fe} nm) sample and a control sample Pt (4 nm)/Fe (t_{Fe}).

Published under an exclusive license by AIP Publishing

compensation point ($x_M \approx 47$), which is in sharp contrast to the behavior observed for HM/FM bilayers in which H_{DL} is proportional to $1/M_s$. H_{DL} reverses sign between x_M and the angular momentum compensation point ($x_A \approx 38$, see below).

Using the obtained H_{DL} values, we calculate ξ^j_{DL} of these FeTb single layers following

$$\xi^j_{DL} \equiv j_s/j = (2e/\hbar)H_{DL}M_s t/j, \quad (3)$$

where e is the elementary charge, $\hbar$ is the reduced Plank's constant, M_s is the saturation magnetization of the spin current detector, t is the thickness of the spin current detector, j_s is the spin current density absorbed by the spin current detector, and $j = E/\rho_{xx}$ is the current density in the spin current generator with electrical resistivity ρ_{xx} (supplementary material, Fig. S10). As we justify in the supplementary material, Sec. 10, Eq. (3) holds for FIMs regardless of the sign of effective gyromagnetic ratio (γ_{eff}). As plotted in Fig. 2(e), ξ^j_{DL} of the 20 nm FeTb first increases rapidly from +0.11 at $x = 29$ to +0.41 at $x = 37$, then (like H_{DL}) suddenly becomes negative for $38 < x < 47$, and finally becomes positive again and starts to decrease from the value +0.16 at $x = 49$ upon further increase in x (see the supplementary material, Sec. 11, for more details of the torque determination). This sign reversal of the dampinglike spin–orbit torque is reaffirmed by the opposite polarity of the current-induced magnetization switching of the $Fe_{57}Tb_{43}$ and the $Fe_{67}Tb_{33}$ (supplementary material, Sec. 16). We find that the sign reversal appears to be correlated with that of the angular momentum. In Fig. 2(f), we show the effective gyromagnetic ratio for the 20 nm FeTb with different compositions as calculated using the relation[39–41] $\gamma_{eff} = (m_{Fe} - m_{Tb})/(m_{Fe}/|\gamma_{Fe}| - m_{Tb}/|\gamma_{Tb}|)$, the magnetic moments of the two sublattices $m_{Fe} = (1 - 0.01x)M_{Fe}$ and $m_{Tb} = 0.01xM_{Tb}$, and the individual gyromagnetic ratios $\gamma_{Fe} = -2.1\mu_B/\hbar$[42] and $\gamma_{Tb} = -1.5\mu_B/\hbar$.[43] The composition of the angular momentum compensation point, where the total angular momentum $S = m_{Fe}/|\gamma_{Fe}| - m_{Tb}/|\gamma_{Tb}|$ is zero, is estimated to be $x_A \approx 38.5$ for the 20 nm FeTb at the room temperature. We note that γ_{eff}, x_A, and x_M in Figs. 2(d)–2(f) are only the 20 nm FeTb samples and different from that for the thicker films [e.g., for the films in Fig. 2(g), $x_A < x_M < 43$]. The FeTb also shows a field-like torque that is relatively small compared to the damping-like torque [supplementary material, Fig. S12].

BULK CHARACTERISTICS AND MICROSCOPIC ORIGIN

To analyze these data, we first show that the strong damping-like torque we observe within FeTb is a bulk effect. Qualitatively similar to previous measurements of CoPt single layers,[26] ξ^j_{DL} of the FeTb layers increases linearly with layer thickness when the thickness is greater than about 40 nm as shown in Fig. 2(g) for $Fe_{57}Tb_{43}$, yielding in the bulk limit a SOT efficiency per thickness of $\xi^j_{DL}/t = 0.036 \pm 0.008\,nm^{-1}$. This behavior is not consistent with an interfacial torque, for which ξ^j_{DL} should be approximately independent of the magnetic-layer thickness.[24,44] We also find that this torque is insensitive to the details of the sample interfaces because we measure essentially the same value of ξ^j_{DL} from symmetric MgO/$Fe_{61}Tb_{39}$ 20 nm/MgO samples and asymmetric SiO_2/$Fe_{61}Tb_{39}$ 20 nm/MgO samples. We, thus, conclude from these characteristics that the damping-like spin torque in FeTb single layers is a bulk effect. This bulk torque is microscopically distinct from the previously reported "interface-engineered" self-torque concluded from a study of GdFeCo.[22]

We suggest that the source of the strong damping-like SOT in the perpendicularly magnetized FeTb is most likely a strong conventional bulk spin Hall effect (SHE). We have considered the possibility of origins associated with the anomalous Hall effect or planar Hall effect, but these can only generate spin polarization collinear with the magnetization.[45–47] Magnetic and antiferromagnetic spin Hall effects[48,49] are also not relevant because they are odd under time reversal, while we find that the damping-like torque efficiencies generated in FeTb for a given applied electric field do not reverse orientation when the magnetization reverses. We have further verified the existence of a strong SHE in FeTb by measuring the spin current emitted by FeTb layers. We performed thickness-dependent spin-torque ferromagnetic resonance (ST-FMR) experiments[50,51] on a control sample of $Fe_{50}Tb_{50}$ (20 nm)/Ti (1 nm)/Fe (3.8–10.5 nm) and used the in-plane magnetized Fe layer to detect the spin current emitted from the FeTb [Fig. 2(h)]. Here, the 1 nm Ti spacer layer was used to suppress the exchange coupling between the FeTb and the Fe layers [supplementary material, Fig. S13(b)]. The PMA FeTb produces no measurable FMR excitation under the condition of small in-plane magnetic field, so the ST-FMR signal we measure from the FeTb/Ti/Fe trilayers corresponds only to magnetic dynamics from the Fe layer. If we define the apparent FMR spin-torque efficiency (ξ_{FMR}) from the ratio of the symmetric and anti-symmetric components of the magnetoresistance response of the ST-FMR (supplementary material, Sec. 13), the actual efficiency of the damping-like torque acting on the Fe layer due to the spin current emitted by the $Fe_{50}Tb_{50}$ ($\xi^j_{DL,ext}$) can be determined by the method of Ref. 51 based on the y-axis intercept in a linear fit of $1/\xi_{FMR}$ vs $1/t_{Fe}$. As shown in Fig. 2(i), we measure $\xi^j_{DL,ext} = 0.16 \pm 0.02$ for $Fe_{50}Tb_{50}$/Ti/Fe, which is three times stronger than that of Pt/Fe bilayers [0.051 ± 0.002, also shown in Fig. 2(i)] for Pt with a resistivity of 38 $\mu\Omega$ cm. We have also measured $\xi^j_{DL,ext}$ for $x = 43$ (where ξ^j_{DL} is negative) and for $x = 29$ (on the other side of the angular momentum compensation point where ξ^j_{DL} is positive again), and we find that the sign of $\xi^j_{DL,ext}$ is unambiguously positive at all three concentrations. The value of $\xi^j_{DL,ext}$ that we quote for $Fe_{50}Tb_{50}$ only represents a lower bound for the internal value of the spin Hall ratio because the torque applied to the Fe is reduced by spin attenuation in the Ti spacer[26,52] interfacial spin backflow[11] and spin memory loss.[53] Spin memory loss, in particular, should be significant at the Ti/Fe interface because it possesses strong interfacial spin–orbit coupling[11] as indicated by the large interfacial magnetic anisotropy energy density of $1.43 \pm 0.05\,erg/cm^2$ (supplementary material, Sec. 14).

A non-zero SOT in a single magnetic layer requires that the sample structure is not symmetric relative to a mirror parallel to the sample plane.[16,26] The required broken symmetry within the FeTb layers seems unrelated to any vertical composition gradient because there is no evidence of a composition gradient in the EELS studies of our films. We also find that a deliberately introduced vertical composition gradient does not enhance the damping-like torque in FeTb. A control sample of 20 nm thick $Fe_{100-x}Tb_x$ in which x varied from 27 to 41 with thickness gave ξ^j_{DL} of 0.05 ± 0.01 (supplementary material, Fig. S15), which is similar to the averaged value of whole film over the thickness using the composition-dependent values in Fig. 2(e), but significantly smaller in magnitude than −0.46 for 20 nm $Fe_{61}Tb_{39}$. In addition, the source of the symmetry breaking is not a vertical thermal gradient because the magnitude of H_{DL} scales in proportion to the applied electric field (supplementary material, Fig. S7), and thus, ξ^j_{DL} is

Published under an exclusive license by AIP Publishing

independent of the applied electric field (symmetry breaking due to Joule heating would give $\xi^j_{DL} \propto E^2$).

STRONG COMPOSITION DEPENDENCE AND SIGN CHANGE

We now turn to analyze the dependence on x of the bulk anti-damping spin torque efficiency ξ^j_{DL} for $Fe_{100-x}Tb_x$ [Fig. 2(e)]. We observe that $|\xi^j_{DL}|$ for the 20 nm $Fe_{100-x}Tb_x$ samples shows a broad peak around $x = 43$, suggesting an enhanced SHE in the intermediate composition range, near and between the two compensation points for magnetization and angular momentum. $|\xi^j_{DL}|$ reaches 0.5 for 20 nm $Fe_{57}Tb_{43}$ films and 3 for 90 nm $Fe_{57}Tb_{43}$ films. Our result differs from the case of GdFeCo, which was reported to have zero self-torque at the compensation point of angular momentum in a previous temperature-dependence study.[22]

The sign change of ξ^j_{DL} that we observe in the 20 nm $Fe_{100-x}Tb_x$ samples between the compensation points for magnetization and angular momentum appears to be correlated with the relative orientation of the magnetization and angular momentum vector. Outside the region between the two compensation points, the magnetization ($m_{Fe} - m_{Tb}$) and angular momentum ($s_{Fe} - s_{Tb}$) are antiparallel ($\gamma_{eff} < 0$), but between the compensation points, the total magnetization becomes parallel to the total angular momentum ($\gamma_{eff} > 0$). A change in the sign of ξ^j_{DL} indicates a change in the sign of the spin angular momentum being transferred to the magnet. However, our ST-FMR measurements on $Fe_{100-x}Tb_x$/Ti/Fe indicate no sign change in the polarization of the spin current emitted from FeTb regardless of composition. The microscopic origin of the sign change of ξ^j_{DL} remains a puzzle and worth study in the future.

PRACTICAL IMPACT AND SELF-TORQUE-DRIVEN MAGNETIZATION SWITCHING

From the technological point of view, a strong bulk torque can be advantageous by itself or in combination with interface-applied torques for applications, such as perpendicular magnetic recording and chiral domain wall/skyrmion devices, that require relatively large thickness for high thermal stability. The damping-like SOT efficiency per unit thickness that we measure in the bulk limit for $Fe_{57}Tb_{43}$, $\xi^j_{DL}/t \approx 0.036\,nm^{-1}$, is much greater than previous reports for other magnetic single layers, e.g., $\sim 0.0017\,nm^{-1}$ for in-plane

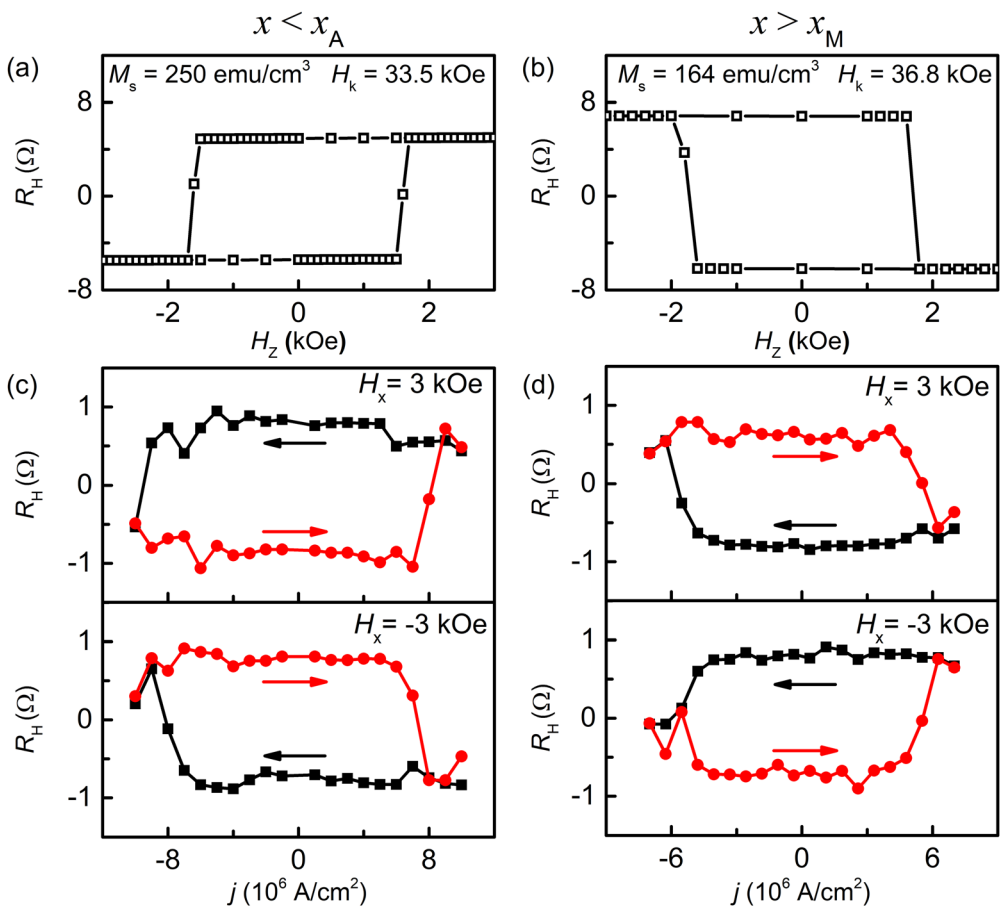

FIG. 3. Anomalous Hall resistance hysteresis of (a) a 20 nm thick $Fe_{67}Tb_{33}$ single layer ($x < x_A$, Fe-dominated, $M_s = 250$ emu/cm^3, $H_k = 33.5$ kOe, and $H_c = 1.59$ kOe) and (b) a 20 nm thick $Fe_{42}Tb_{58}$ single layer ($x > x_M$, Tb-dominated, $M_s = 164$ emu/cm^3, $H_k = 17.5$ kOe, and $H_c = 1.72$ kOe). Current induced magnetization switching of (c) the $Fe_{67}Tb_{33}$ and (d) the $Fe_{42}Tb_{58}$, under a constant in-plane bias field $H_x = \pm 3$ kOe that overcomes the DMI field within the domain walls.

Published under an exclusive license by AIP Publishing

NiFe,[25] $\sim -0.008\,\mathrm{nm}^{-1}$ for in-plane CoPt,[26] $\sim 0.005\,\mathrm{nm}^{-1}$ for in-plane FePt,[16] and $\sim 0.016\,\mathrm{nm}^{-1}$ for perpendicular GdFeCo.[22] Here, we do not compare our ξ^j_{DL}/t result with those out-of-plane HHVR results obtained by applying a large "planar Hall correction" (e.g., $0.045\,\mathrm{nm}^{-1}$ for $L1_0$-FePt single crystals in Ref. 19) because, as we noted above, the planar Hall correction is generally found to give incorrect values when it is not negligible.[36–38]

The bulk SOT of FeTb is sufficiently strong to drive SOT switching of layers with very large thicknesses and strong PMA. In Figs. 3(a)–3(d), we compare magnetic-field-driven switching and SOT switching for both a 20 nm $Fe_{67}Tb_{33}$ device ($x < x_A$, Fe-dominated, $M_s = 250\,\mathrm{emu/cm^3}$, $H_k = 33.5\,\mathrm{kOe}$, and $H_c = 1.59\,\mathrm{kOe}$) and a 20 nm $Fe_{42}Tb_{58}$ device ($x > x_M$, Tb-dominated, $M_s = 164\,\mathrm{emu/cm^3}$, $H_k = 17.5\,\mathrm{kOe}$, and $H_c = 1.72\,\mathrm{kOe}$) as two representative examples. Figures 3(a) and 3(b) show the Hall resistance (R_H) of the samples as a function of H_z, which indicate sharp full switching for both samples with $\Delta R_H = 2\,R_{AHE} = +11\,\Omega$ ($-12.2\,\Omega$) for the Fe- (Tb-)dominated sample. In Figs. 3(c) and 3(d), we show R_H of the two samples measured following the application of sequences of current pulses of different amplitudes (in duration) under the application of a constant symmetry-breaking in-plane bias field H_x along the current direction (x direction). We measure a switching current density of only $(8.2 \pm 1.2) \times 10^6$ A/cm^2 for the 20 nm $Fe_{67}Tb_{33}$ and $(5.5 \pm 0.2) \times 10^6$ A/cm for the 20 nm $Fe_{39}Tb_{61}$. The current-driven switching is only partial ($\sim$16% of the full value of ΔR_H for magnetic-field-driven switching), likely because the non-uniform pinning impedes free motion of domain walls in this domain-wall-mediated switching regime. Full current-driven reversal is likely still possible in nanodot devices with improved magnetic homogeneity as recently demonstrated in CuPt/CoPt bilayers.[54] Here, the switching chirality is opposite for the Fe-dominated $Fe_{67}Tb_{33}$ and Tb-dominated $Fe_{42}Tb_{58}$, i.e., clockwise (anti-clockwise) for the former but anti-clockwise (clockwise) for the latter when $H_x < 0$ ($H_x > 0$) [Figs. 3(c) and 3(d)]. This is because the SOT fields are of the same sign for the two samples ($\xi^j_{DL} > 0$), but the anomalous Hall resistances are of opposite signs ($\Delta R_H > 0$ for $Fe_{67}Tb_{33}$ but <0 for $Fe_{42}Tb_{58}$). We also note that the 20 nm $Fe_{57}Tb_{43}$ ($x_A < x < x_M$, $\Delta R_H > 0$, $\xi^j_{DL} < 0$) can also be switched at a low current density of $(5.5 \pm 0.1) \times 10^6$ A/cm [supplementary material, Fig. S16(c)], but the switching polarity is opposite to that of the $Fe_{67}Tb_{33}$ ($x < x_A$, $\Delta R_H > 0$, $\xi^j_{DL} > 0$) due to the negative sign of the bulk spin–orbit torque in the $Fe_{57}Tb_{43}$.

CONCLUSION

We have demonstrated a giant damping-like SOT arising from the SHE in composition-uniform, amorphous, and sputter-deposited ferrimagnetic $Fe_{100-x}Tb_x$ single layers with giant PMA. This bulk torque exhibits no apparent correlation to the interfaces or the absence/presence of a composition gradient. The torque reaches a constant value of efficiency per unit layer thickness in the bulk limit, $\xi^j_{DL}/t \approx 0.036\,\mathrm{nm}^{-1}$. This is more than twice greater any previous report for other magnetic single layers. The torque varies strongly with composition and achieves giant efficiencies $|\xi^j_{DL}|$ of 0.5 for 20 nm $Fe_{61}Tb_{39}$ and 3 for 90 nm $Fe_{57}Tb_{43}$. Interestingly, the torque becomes negative in sign in the intermediate composition range where total angular momentum becomes parallel to the magnetization rather than antiparallel. We also show that the bulk SOT can drive switching in tens of nm thick FeTb layers with strong PMA and high coercivity. For example, the bulk SOT can switch a 20 nm FeTb at very low current densities of a few MA/cm^2. Our findings of giant bulk SOT efficiency and intriguing torque-compensation correlation will stimulate study of such unique spin–orbit phenomena in a variety of ferrimagnetic hosts. Our work suggests a promising strategy for self-driven-switching perpendicular ferrimagnetic devices with low power, high density, and straightforward integration with CMOS circuits because there is no requirement for epitaxy or composition gradient.

SUPPLEMENTARY MATERIAL

See the supplementary material for more details on sample fabrication and characterizations, thickness gradient of FIB-thinned STEM samples, magnetic properties of $Fe_{100-x}Tb_x$ single layers, Anomalous Hall resistance and coercivity of $Fe_{100-x}Tb_x$ single layer, estimation of current-induced temperature increase, subtraction of effects of anomalous Nernst voltage from harmonic Hall voltage response, coherent rotation at small polar angles, validation of Eq. (3) in the main text planer Hall resistance, resistivity of the 20 nm $Fe_{100-x}Tb_x$, raw data for representative samples exhibiting different torque signs, field-like spin-orbit torque in $Fe_{100-x}Tb_x$ single layer, spin-torque ferromagnetic resonance measurements, interfacial perpendicular magnetic anisotropy energy density, HHVR measurement of a 20 nm thick composition-gradient $Fe_{100-x}Tb_x$ ($x = 27 \rightarrow 41$), and more examples of magnetization switching by the bulk spin-orbit torque.

ACKNOWLEDGMENTS

The authors thank Robert A. Buhrman for support. This work was funded in part by the Office of Naval Research (No. N00014-19-1-2143), in part by the Defense Advanced Research Projects Agency (No. D18AC00009), and in part by the NSF Materials Research Science and Engineering Center Program (No. DMR-1719875) through the Cornell Center for Materials Research. Device fabrication was performed at the Cornell Nanofabrication Facility, in part by the NSF (No. NNCI-2025233) as part of the National Nanotechnology Coordinated Infrastructure, and in part by the Strategic Priority Research Program of the Chinese Academy of Sciences (No. XDB44000000). Q.L. acknowledges the financial support by the China Scholarship Council (File No. 201906460052). L.Z. acknowledges the start-up funding support from Institute of Semiconductors, Chinese Academy of Sciences (E2SEBB01).

AUTHOR DECLARATIONS

Conflict of Interest

The authors have no conflicts to disclose.

Author Contributions

Q.L. and L.Z. contributed equally to this work.

DATA AVAILABILITY

The data that support the findings of this study are available from the corresponding author upon reasonable request.

REFERENCES

[1] C. Kaiser, A. F. Panchula, and S. S. P. Parkin, Phys. Rev. Lett. **95**, 047202 (2005).
[2] H. Awano, J. Magn. Magn. Mater. **383**, 50 (2015).

Published under an exclusive license by AIP Publishing

[3]N. Roschewsky, T. Matsumura, S. Cheema, F. Hellman, T. Kato, S. Iwata, and S. Salahuddin, Appl. Phys. Lett. **109**, 112403 (2016).
[4]J. Finley, C. Lee, P. Y. Huang, and L. Liu, Adv. Mater. **31**, 1805361 (2019).
[5]K. Kim, S. K. Kim, Y. Hirata, S. Oh, T. Tono, D. Kim, T. Okuno, W. S. Ham, S. Kim, G. Go, Y. Tserkovnyak, A. Tsukamoto, T. Moriyama, K. Lee, and T. Ono, Nat. Mater. **16**, 1187 (2017).
[6]K. Cai, Z. Zhu, J. M. Lee, R. Mishra, L. Ren, S. D. Pollard, P. He, G. Liang, K. L. Teo, and H. Yang, Nat. Electron. **3**, 37 (2020).
[7]L. Caretta, M. Mann, F. Büttner, K. Ueda, B. Pfau, C. M. Günther, P. Hessing, A. Churikova, C. Klose, M. Schneider, D. Engel, C. Marcus, D. Bono, K. Bagschik, S. Eisebitt, and G. S. D. Beach, Nat. Nanotechnol. **13**, 1154 (2018).
[8]F. Radu and J. Sánchez-Barriga, *Novel Magnetic Nanostructures* (Elsevier, 2018), pp. 267–331.
[9]Z. Zhang, Z. Zheng, Y. Zhang, J. Sun, K. Lin, K. Zhang, X. Feng, L. Chen, and J. Wang, IEEE Electron Device Lett. **42**, 152–155 (2021).
[10]H. Wu, Y. Xu, P. Deng, Q. Pan, S. A. Razavi, K. Wong, L. Huang, B. Dai, Q. Shao, G. Yu, X. Han, J.-C. Rojas-Sánchez, S. Mangin, and K. L. Wang, Adv. Mater. **31**, 1901681 (2019).
[11]L. Zhu, D. C. Ralph, and R. A. Buhrman, Appl. Phys. Rev. **8**, 031308 (2021).
[12]N. Roschewsky, C. Lambert, and S. Salahuddin, Phys. Rev. B **96**, 064406 (2017).
[13]J. Finley and L. Q. Liu, Phys. Rev. Appl. **6**, 054001 (2016).
[14]K. Ueda, M. Mann, P. W. P. de Brouwer, D. Bono, and G. S. D. Beach, Phys. Rev. B **96**, 064410 (2017).
[15]J. Han, A. Richardella, S. A. Siddiqui, J. Finley, N. Samarth, and L. Liu, Phys. Rev. Lett. **119**, 077702 (2017).
[16]L. Zhu, D. C. Ralph, and R. A. Buhrman, Adv. Funct. Mater. **31**, 2103898 (2021).
[17]M. Jiang, H. Asahara, S. Sato, T. Kanaki, H. Yamasaki, S. Ohya, and M. Tanaka, Nat. Commun. **10**, 2590 (2019).
[18]L. Liu, J. Yu, R. González-Hernández, C. Li, J. Deng, W. Lin, C. Zhou, T. Zhou, J. Zhou, H. Wang, R. Guo, H. Y. Yoong, G. M. Chow, X. Han, B. Dupé, J. Železný, J. Sinova, and J. Chen, Phys. Rev. B **101**, 220402 (2020).
[19]M. Tang, K. Shen, S. Xu, H. Yang, S. Hu, W. Lü, C. Li, M. Li, Z. Yuan, S. J. Pennycook, K. Xia, A. Manchon, S. Zhou, and X. Qiu, Adv. Mater. **32**, 2002607 (2020).
[20]J. W. Lee, J. Y. Park, J. M. Yuk, and B. Park, Phys. Rev. Appl. **13**, 044030 (2020).
[21]R. Q. Zhang, L. Y. Liao, X. Z. Chen, T. Xu, L. Cai, M. H. Guo, H. Bai, L. Sun, F. H. Xue, J. Su, X. Wang, C. H. Wan, H. Bai, Y. X. Song, R. Y. Chen, N. Chen, W. J. Jiang, X. F. Kou, J. W. Cai, H. Q. Wu, F. Pan, and C. Song, Phys. Rev. B **101**, 214418 (2020).
[22]D. Céspedes-Berrocal, H. Damas, S. Petit-Watelot, D. Maccariello, P. Tang, A. Arriola-Córdova, P. Vallobra, Y. Xu, J. Bello, E. Martin, S. Migot, J. Ghanbaja, S. Zhang, M. Hehn, S. Mangin, C. Panagopoulos, V. Cros, A. Fert, and J. Rojas-Sánchez, Adv. Mater. **33**, 2007047 (2021).
[23]H. Kurebayashi, J. Sinova, D. Fang, A. C. Irvine, T. D. Skinner, J. Wunderlich, V. Novák, R. P. Campion, B. L. Gallagher, E. K. Vehstedt, L. P. Zârbo, K. Výborný, A. J. Ferguson, and T. Jungwirth, Nat. Nanotechnol. **9**, 211 (2014).
[24]Z. Luo, Q. Zhang, Y. Xu, Y. Yang, X. Zhang, and Y. Wu, Phys. Rev. Appl. **11**, 064021 (2019).
[25]W. Wang, T. Wang, V. P. Amin, Y. Wang, A. Radhakrishnan, A. Davidson, S. R. Allen, T. J. Silva, H. Ohldag, D. Balzar, B. L. Zink, P. M. Haney, J. Q. Xiao, D. G. Cahill, V. O. Lorenz, and X. Fan, Nat. Nanotechnol. **14**, 819 (2019).
[26]L. Zhu, X. S. Zhang, D. A. Muller1, D. C. Ralph, and R. A. Buhrman, Adv. Funct. Mater. **30**, 2005201 (2020).
[27]S. Bals, W. Tirry, R. Geurts, Z. Yang, and D. Schryvers, Microsc. Microanal. **13**, 80 (2007).
[28]A. Hassdenteufel, B. Hebler, C. Schubert, A. Liebig, M. Teich, M. Helm, M. Aeschlimann, M. Albrecht, and R. Bratschitsch, Adv. Mater. **25**, 3122 (2013).
[29]T. Ruckert, J. Tappert, R. A. Brand, and W. Keune, J. Magn. Magn. Mater. **165**, 411 (1997).
[30]B. Hebler, A. Hassdenteufel, P. Reinhardt, H. Karl, and M. Albrecht, Front. Mater. **3**, 8 (2016).
[31]S. A. Siddiqui, J. Han, J. T. Finley, C. A. Ross, and L. Liu, Phys. Rev. Lett. **121**, 057701 (2018).
[32]Y. Xu, D. Chen, S. Tong, H. Chen, X. Qiu, D. Wei, and J. Zhao, Phys. Rev. Appl. **14**, 034064 (2020).
[33]A. Ghosh, K. Garello, C. O. Avci, M. Gabureac, and P. Gambardella, Phys. Rev. Appl. **7**, 014004 (2017).
[34]H. Yang, H. Chen, M. Tang, S. Hu, and X. Qiu, Phys. Rev. B **102**, 024427 (2020).
[35]M. Hayashi, J. Kim, M. Yamanouchi, and H. Ohno, Phys. Rev. B **89**, 144425 (2014).
[36]L. Zhu, K. Sobotkiewich, X. Ma, X. Li, D. C. Ralph, and R. A. Buhrman, Adv. Funct. Mater. **29**, 1805822 (2019).
[37]J. Torrejon, J. Kim, J. Sinha, S. Mitani, M. Hayashi, M. Yamanouchi, and H. Ohno, Nat. Commun. **5**, 4655 (2014).
[38]S. Karimeddiny, T. M. Cham, D. C. Ralph, and Y. K. Luo, arXiv:2109.13759 (2021).
[39]M. Binder, A. Weber, O. Mosendz, G. Woltersdorf, M. Izquierdo, I. Neudecker, J. R. Dahn, T. D. Hatchard, J.-U. Thiele, C. H. Back, and M. R. Scheinfein, Phys. Rev. B **74**, 134404 (2006).
[40]C. D. Stanciu, A. V. Kimel, F. Hansteen, A. Tsukamoto, A. Itoh, A. Kirilyuk, and T. Rasing, Phys. Rev. B **73**, 220402 (2006).
[41]X. Jiang, L. Gao, J. Z. Sun, and S. S. P. Parkin, Phys. Rev. Lett. **97**, 217202 (2006).
[42]B. I. Min and Y. R. Jang, J. Phys.: Condens. Matter **3**, 5131 (1991).
[43]Y. Ogata, H. Chudo, M. Ono, K. Harii, M. Matsuo, S. Maekawa, and E. Saitoh, Appl. Phys. Lett. **110**, 072409 (2017).
[44]S. Emori, T. Nan, A. M. Belkessam, X. Wang, A. D. Matyushov, C. J. Babroski, Y. Gao, H. Lin, and N. X. Sun, Phys. Rev. B **93**, 180402(R) (2016).
[45]T. Taniguchi, J. Grollier, and M. D. Stiles, Phys. Rev. Appl. **3**, 044001 (2015).
[46]C. Qin, S. Chen, Y. Cai, F. Kandaz, and Y. Ji, Phys. Rev. B **96**, 134418 (2017).
[47]C. Safranski, E. A. Montoya, and I. N. Krivorotov, Nat. Nanotechnol. **14**, 27 (2019).
[48]M. Kimata, H. Chen, K. Kondou, S. Sugimoto, P. K. Muduli, M. Ikhlas, Y. Omori, T. Tomita, A. H. MacDonald, S. Nakatsuji, and Y. Otani, Nature **565**, 627 (2019).
[49]X. Chen, S. Shi, G. Shi, X. Fan, C. Song, X. Zhou, H. Bai, L. Liao, Y. Zhou, H. Zhang, A. Li, Y. Chen, X. Han, S. Jiang, Z. Zhu, H. Wu, X. Wang, D. Xue, H. Yang, and F. Pan, Nat. Mater. **20**, 800 (2021).
[50]L. Liu, T. Moriyama, D. C. Ralph, and R. A. Buhrman, Phys. Rev. Lett. **106**, 036601 (2012).
[51]C. Pai, Y. Ou, L. H. Vilela-Leão, D. C. Ralph, and R. A. Buhrman, Phys. Rev. B **92**, 064426 (2015).
[52]P. M. Haney, H. W. Lee, K. J. Lee, A. Manchon, and M. D. Stiles, Phys. Rev. B **87**, 174411 (2013).
[53]L. Zhu, D. C. Ralph, and R. A. Buhrman, Phys. Rev. Lett. **122**, 077201 (2019).
[54]L. Liu, C. Zhou, X. Shu, C. Li, T. Zhao, W. Lin, J. Deng, Q. Xie, S. Chen, J. Zhou, R. Guo, H. Wang, J. Yu, S. Shi, P. Yang, S. Pennycook, A. Manchon, and J. Chen, Nat. Nanotechnol. **16**, 277 (2021).

Published under an exclusive license by AIP Publishing